JMEPEG (2006) 15:394-398
DOI: 10.1361/105994906X117170

1059-9495/$19.00

Effect of Manganese Addition on Reactive Evaporation of Chromium in Ni-Cr Alloys

Gordon R. Holcomb and David E. Alman

(Submitted January 16, 2006; in revised form May 18, 2006)

Chromium is used as an alloy addition in stainless steels and nickel-chromium alloys to form protective chromium oxide scales. Chromium oxide undergoes reactive evaporation in high-temperature exposures in the presence of oxygen and/or water vapor. Deposition of gaseous chromium species onto solid oxide fuel-cell electrodes can reduce the efficiency of the fuel cell. Manganese additions to the alloy can reduce the activity of chromium in the oxide, either from solid solution replacement of chromium with manganese (at low levels of manganese) or from the formation of manganese-chromium spinels (at high levels of manganese). This reduction in chromium activity leads to a predicted reduction in chromium evaporation factors as much as 35 at 800 °C and 55 at 700 °C. Quantifying the effects of manganese additions on chromium evaporation should aid alloy development of metallic interconnects and balance-of-plant alloys.

Keywords chromium, evaporation, interconnect, manganese, solid oxide fuel cell, spinel

1. Introduction

Deposition of chromium onto solid oxide fuel-cell (SOFC) electrodes is widely viewed as a major source of efficiency loss in fuel cells (Ref 1-3). Chromium-bearing alloys, used as metallic interconnects or upstream in the balance of plant (BOP), form protective scales that contain chrome oxides. When chromium in the chrome oxides undergoes reactive evaporation in the presence of O_2 or H_2O, then chromium exists in the gas phase and is available for deposition on the SOFC electrodes. An example of a reactive evaporation reaction is Eq 1.

$$½Cr_2O_3(s) + ¾O_2(g) = CrO_3(g) \quad \text{(Eq 1)}$$

Equation 1 describes formation of $CrO_3(g)$, which is the most prevalent chrome oxide gas species in the absence of water vapor. The vapor pressure of $CrO_3(g)$ is related to the activity of chromia (Cr_2O_3). Alloying elements in the alloy can lower the activity of Cr_2O_3, for example, by substitution of Ni or Mn for Cr or by formation of $MnCr_2O_4$ spinel. The spinel is essentially a matrix of Cr_2O_3 and MnO.

In the case of alloying with Mn, the reduction of chromia activity, and thus the reduction of chrome evaporation, would be at a maximum when sufficient Mn is available, such that a continuous layer of spinel forms on the surface of the protective oxide. Smaller amounts of Mn would result in smaller reductions in chromia activity but would still be of benefit. Too much Mn can be detrimental from the viewpoints of oxidation and physical properties; thus, the goal herein is to quantify the benefits of Mn addition so that alloy design for metallic interconnects or upstream BOP can optimize Mn content in the alloy.

The effectiveness of reducing the amount of chromium deposition onto SOFC electrodes is examined first from a theoretical basis by comparing the evaporation and thermodynamics of reactive evaporation from Cr_2O_3 with that from $MnCr_2O_4$. Second, long-term oxidation experiments were conducted on a series of Ni-25Cr-0.01Y-*x*Mn alloys to indirectly measure the evaporation rate. Improvements in measuring the evaporation rate, using transport methods, are introduced.

1.1 Evaporation

Reactive evaporation of Cr_2O_3 (or $MnCr_2O_4$) can be modeled in a variety of ways. The maximum evaporation rate can be found from the Knudsen effusion (Ref 4), Eq 2.

$$\text{Evaporation}\left(\frac{\text{g}}{\text{cm}^2\,\text{s}}\right) = \frac{m}{tA} = p\sqrt{\frac{M}{2\pi RT}} = 44.33\,p\sqrt{\frac{M}{T}} \quad \text{(Eq 2)}$$

where m is the mass of the vapor generated (g), t is time (s), A is surface area (cm^2), p is vapor pressure (atm), M is the molecular mass of the vapor (g/mol), T is temperature (K), and R is the gas constant. Thus, the evaporation rate is proportional to the vapor pressure of the gas species.

Real evaporation rates can be many orders of magnitude lower than maximum evaporation rates. One way to determine the real evaporation rates is to assume that volatility is limited by the transport of the volatile species through a laminar boundary layer in the gas phase. For flat-plate geometry, the evaporation rate can be calculated by Eq 3 (Ref 5, 6):

$$\text{Evaporation}\left(\frac{\text{g}}{\text{cm}^2\,\text{h}}\right) = 0.664\text{Re}^{0.5}\,\text{Sc}^{0.33}D\rho L^{-1} \quad \text{(Eq 3)}$$

where Re and Sc are the dimensionless Reynolds and Schmidt numbers, D and ρ are the interdiffusion coefficient and density of the volatile specie in the boundary layer, respectively, and L

This paper was presented at the ASM Materials Solutions Conference & Show held October 18-21, 2004 in Columbus, OH.

Gordon R. Holcomb and **David E. Alman,** National Energy Technology Laboratory, 1450 Queen Ave. SW, Albany, OR 97321. Contact e-mail: gordon.holcomb@netl.doe.gov.

is the characteristic length of the flat plate. When simplified (Ref 5), Eq 3 becomes:

$$\text{Evaporation}\left(\frac{\text{g}}{\text{cm}^2\,\text{h}}\right) \propto \frac{v^{0.5}}{P_{\text{T}}^{0.5}}p \qquad \text{(Eq 4)}$$

for low- to moderate-flow conditions and

$$\text{Evaporation}\left(\frac{\text{g}}{\text{cm}^2\,\text{h}}\right) \propto \frac{v^{0.8}}{P_{\text{T}}^{0.2}}p \qquad \text{(Eq 5)}$$

for turbulent high-flow conditions ($\text{Re} > 3 \times 10^5$). In Eq 4 and 5, v is the linear gas velocity, P_{T} is the total pressure, and p is the partial pressure of the evaporative gas species. As with the maximum evaporation rate of Eq 2, Eq 4 and 5 also show the evaporation rate proportional to p. Thus, the thrust of the thermodynamic treatment is determination of the partial pressures of the evaporating gas species.

1.2 Thermodynamics

A multitude of possible chromium-containing gas species can be formed from O_2 and H_2O. These include Cr, Cr_2, CrH, CrO, CrO_2, CrO_3, CrOH, $Cr(OH)_2$, $Cr(OH)_3$, $Cr(OH)_4$, CrO(OH), $CrO(OH)_2$, $CrO(OH)_3$, $CrO(OH)_4$, $CrO_2(OH)$, and $CrO_2(OH)_2$. The most important of these, in terms of highest partial pressures, are CrO_3, $CrO_2(OH)_2$, and $CrO_2(OH)$.

The Gibbs energy of formation, ΔG_f, of each gas species is used to determine its partial pressure over either Cr_2O_3 or $MnCr_2O_4$. For example, for the formation of CrO_3 over Cr_2O_3, Eq 1, the partial pressure of $CrO_3(g)$, P_{CrO3}, can be found from Eq 6:

$$\Delta G_1 = \Delta G_{\text{f,CrO}_3\text{(g)}} - \tfrac{1}{2}\Delta G_{\text{f,Cr}_2\text{O}_3} = -RT \ln \frac{P_{\text{CrO}_3}}{a_{\text{Cr}_2\text{O}_3}^{1/2} P_{\text{O}_2}^{3/4}} \qquad \text{(Eq 6)}$$

For pure Cr_2O_3, the activity of chromia, $a_{Cr_2O_3}$, is equal to 1. Another example is the formation of $CrO_2(OH)_2(g)$ over $MnCr_2O_4$, Eq 7-9:

$$\tfrac{1}{2}\text{MnCr}_2\text{O}_4 + \tfrac{3}{4}\text{O}_2 + \text{H}_2\text{O} = \text{CrO}_2(\text{OH})_2\text{(g)} + \tfrac{1}{2}\text{MnO} \qquad \text{(Eq 7)}$$

$$\Delta G_7 = \Delta G_{\text{f,CrO}_2\text{(OH)}_2\text{(g)}} + \tfrac{1}{2}\Delta G_{\text{f,MnO}} - \tfrac{1}{2}\Delta G_{\text{f,MnCr}_2\text{O}_4} - \Delta G_{\text{f,H}_2\text{O}} \qquad \text{(Eq 8)}$$

$$\Delta G_7 = -RT \ln \frac{P_{\text{CrO}_2\text{(OH)}_2} a_{\text{MnO}}^{1/2}}{a_{\text{MnCr}_2\text{O}_4}^{1/2} P_{\text{O}_2}^{3/4} P_{\text{H}_2\text{O}}} \qquad \text{(Eq 9)}$$

The ΔG_f for $CrO_2(OH)_2(g)$ is not well established. Opila (Ref 5) has reviewed the literature and has found that using data based on Glusko (Ref 7) results in much lower calculated partial pressures of $CrO_2(OH)_2(g)$ than using data based on Ebbinghaus (Ref 8). Glusko is the source of $CrO_2(OH)_2(g)$ data for the ITVAN (Ref 9) and HSC (Ref 10) thermodynamics programs. Opila (Ref 5) also shows that the experimental data of Gindorf et al. (Ref 11) lie between that predicted by Glusko and Ebbinghaus (in terms of log $P_{CrO_2(OH)_2}$). Additionally, initial experimental results from Opila (Ref 12) indicate values

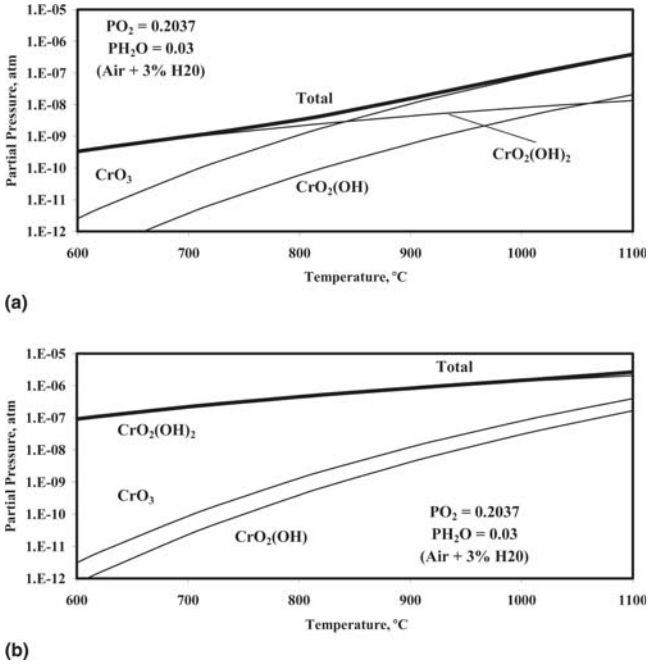

Fig. 1 Partial pressures of $CrO_3(g)$, $CrO_2(OH)_2(g)$, and $CrO_2(OH)(g)$ over pure Cr_2O_3 in air plus 3% H_2O. Thermodynamic data for Cr-containing gas species from (a) Ref 7 and (b) Ref 8

closer to Ebbinghaus. Thus the Glusko (Ref 7) and Ebbinghaus (Ref 8) data sources form lower and upper bounds for predicting evaporation losses.

Using equations similar to Eq 1 and 6, the partial pressures of $CrO_3(g)$, $CrO_2(OH)_2(g)$, and $CrO_2(OH)(g)$ over pure Cr_2O_3 (activity of 1) were found for conditions of $P_{O_2} = 0.2037$ and $P_{H_2O} = 0.03$ (air plus 3% H_2O) and are shown in Fig. 1(a) using the thermodynamic data of the HSC program (Ref 10) (ΔG_f for $CrO_2(OH)_2(g)$ based on Glusko (Ref 7)) and in Fig. 1(b) replacing the ΔG_f for $CrO_3(g)$, $CrO_2(OH)_2(g)$, and $CrO_2(OH)(g)$ with that of Ebbinghaus (Ref 8).

Also shown in Fig. 1 is the total partial pressure of gaseous chromium-containing species. Figure 1 shows a large difference in the total partial pressure of Cr-containing gas species, based primarily on the different thermodynamic data sources for $CrO_2(OH)_2(g)$.

For similar calculations over $MnCr_2O_4$, the difficultly lies in sparse ΔG_f data for $MnCr_2O_4$. Four values of ΔG_f (from Cr_2O_3 and MnO) were found in the literature at higher temperatures, Eq 10-13:

$$\Delta G_{\text{f,MnCr}_2\text{O}_4} = -59.376 \text{ kJ/mol at } 1100\ ^\circ\text{C (Ref 13)} \qquad \text{(Eq 10)}$$

$$\Delta G_{\text{f,MnCr}_2\text{O}_4} = -59.0 \text{ kJ/mol at } 1250\ ^\circ\text{C (Ref 14)} \qquad \text{(Eq 11)}$$

$$\Delta G_{\text{f,MnCr}_2\text{O}_4} = -42.278 \text{ kJ/mol at } 1300\ ^\circ\text{C (Ref 15)} \qquad \text{(Eq 12)}$$

$$\Delta G_{\text{f,MnCr}_2\text{O}_4} = -52.600 \text{ kJ/mol at } 1600\ ^\circ\text{C (Ref 16)} \qquad \text{(Eq 13)}$$

Taken together, the values of Eq 10-13 do not form a consistent relationship with respect to temperature. The values in Eq 10 and 13 were determined by similar methods of spinel-oxide phase equilibria: $MnCr_2O_4$-$CoCr_2O_4$ (Ref 13) and

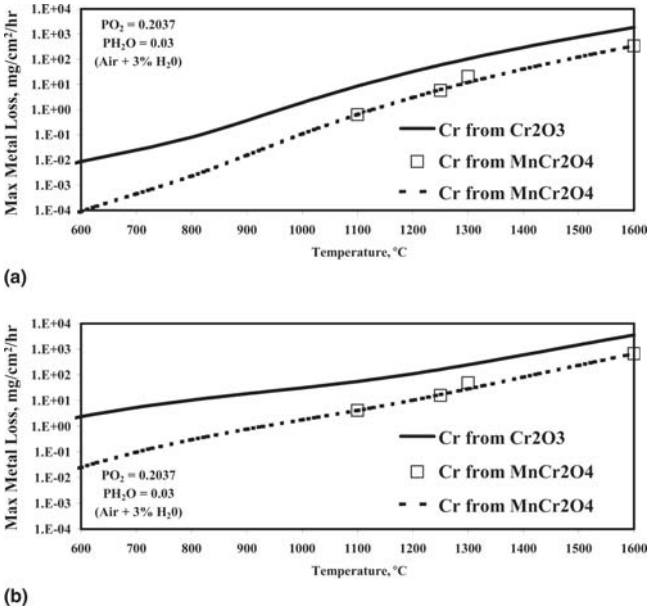

Fig. 2 Maximum evaporation rate of Cr over pure Cr_2O_3 and pure $MnCr_2O_4$ in air plus 3% H_2O. The data points represent the use of ΔG_f data of Eq 10-13 (Ref 13-16). The dotted line represents the use of estimated ΔG_f data as a function of temperature. Thermodynamic data for Cr-containing gas species from (a) Ref 7 and (b) Ref 8

$MnCr_2O_4$-$MnAl_2O_4$ (Ref 16). Consequently, lower temperature values of ΔG_f were estimated using Eq 10 and 13. To make these estimates, the Newmann and Kopp rule (Ref 4) was used where the change in heat capacity, ΔC_p, is equal to zero for condensed reactions. This allows the data in Eq 10 and 12 to be fitted to $\Delta G_T = \Delta H_{298} - T\Delta S_{298}$, where $\Delta H_{298} = -77.985$ kJ/mol and $\Delta S_{298} = -0.0136$ kJ/mol/K.

The total partial pressure of gaseous chromium-containing species over pure $MnCr_2O_4$ was calculated and shown in comparison with the results over Cr_2O_3 (Fig. 2, in terms of maximum evaporation rate instead of total partial pressure). The data points in Fig. 2 represent the use of ΔG_f data of Eq 10-13 (Ref 13-16). The dotted lines in Fig. 2 represent the use of estimated ΔG_f data as a function of temperature. Figure 2(a) uses the thermodynamic data of the HSC program (Ref 10) (ΔG_f for $CrO_2(OH)_2(g)$ based on Glusko [Ref 7]), and Fig. 2(b) uses the ΔG_f for $CrO_3(g)$, $CrO_2(OH)_2(g)$, and $CrO_2(OH)(g)$ of Ebbinghaus (Ref 8).

Figure 2 shows the large reduction in Cr evaporation from a scale consisting of Cr_2O_3 to one having an outer layer of $MnCr_2O_4$. Without a continuous layer of $MnCr_2O_4$, or when the activity of Cr_2O_3 is less than 1 due to Mn additions, the reduction in Cr evaporation would lie between the solid and dotted lines in Fig. 2.

The calculations in Fig. 2 are for an environment of air plus 3% H_2O. When the calculations are repeated for other combinations of P_{O2} and P_{H2O}, the total partial pressure and maximum evaporation rates change significantly, Table 1. The conditions with the largest evaporation rates are when O_2 and H_2O are both present.

Regardless of the values of P_{O_2} and P_{H_2O}, or of the source of the thermodynamic data for $CrO_2(OH)_2(g)$, the ratio of the maximum evaporation rate over a spinel to that over chromia (the reduction factors in Table 1) are only functions of temperature. The reduction factors for $MnCr_2O_4$ range from 18 at 1000 °C to 95 at 600 °C.

2. Experimental Procedures

A series of oxidation experiments were designed to measure the evaporation rates over Ni-25Cr alloys with various amounts of Mn additions. With these evaporation rates, experimental reduction factors could be compared with those calculated from thermodynamics.

The basis of the experiments was to conduct long-term oxidation tests at 950 °C in air plus 5% water vapor until a steady-state scale thickness was reached, and so subsequent mass loss measurements would measure the evaporation rate. Nickel-chromium alloys that form protective scales grow with parabolic kinetics, in which scale growth is inversely proportional to scale thickness. Combining this with constant evaporation rates that are independent of scale thickness, there should come a time where scale growth from oxidation matches scale loss from evaporation, thus producing a steady-state scale thickness. An elevated temperature of 950 °C was used to increase the evaporation to a more readily measurable rate.

Five Ni-25Cr alloys were melted and rolled to have nominal compositions of Ni-25Cr and Ni-25Cr-0.01Y-*x*Mn, with *x* equal to 0, 0.4, 1, and 3. It was thought that scale adhesion could be improved by the addition of a small amount of Y. The actual compositions are shown in Table 2.

The samples were cut into pieces, ~1.5 × 0.9 × 0.3 cm, and the surfaces were ground against 600 grit. The samples were placed inside alumina crucibles and heated to 950 °C in an alumina tube furnace. Water was added to a preheating chamber with a metering pump and fed into the furnace along with air. The gas mixture was nominally 5% water vapor and flowing at ~10 cm/min. Periodically, the furnace was cooled, and samples were removed for weighing and then put back into the furnace to heat back up to temperature. The furnace was heated and allowed to cool at a rate of 200 °C/h.

3. Results

The results of the mass change measurements are shown in Fig. 3. However, the negative slopes for several of the alloys after 500 h do not represent the evaporation rate. The samples were observed spall, with a fine powder collecting inside the crucibles.

Subsequent to the observation of spalling, the total mass of each sample and crucible was collected (Fig. 4). The slopes of the lines continue to either increase or remain flat. The conclusion was that the spalling was continuing and allowing oxidation to occur at a faster rate than evaporation. Thus, the evaporation rate could not be obtained from these results.

3.1 Future Work

A more direct measurement of the evaporation rate is planned using the transpiration method (Ref 4, 11). In this method, chromium gas species are generated from the oxide in a flowing gas stream. The chromium gas species travel through a capillary and collected by condensation outside the furnace. One example of the successful use of this method is by Gindorf et al. (Ref 11), who measured Cr evaporation from the oxide

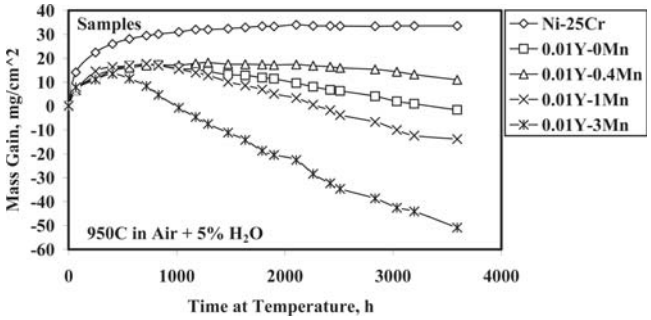

Fig. 3 Mass change with time for the five Ni-25Cr-Y-Mn alloys oxidized in air + 5% H_2O at 950 °C

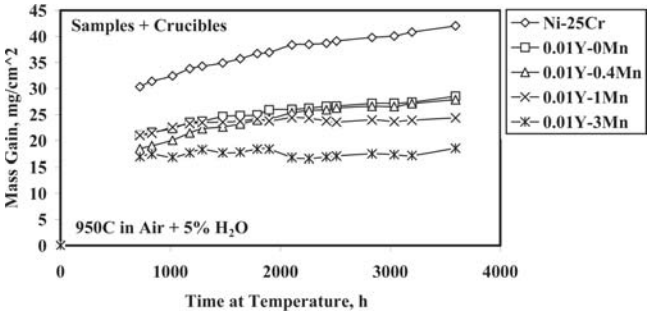

Fig. 4 Mass change with time for the five crucibles plus the Ni-25Cr-Y-Mn alloys oxidized in air + 5% H_2O at 950 °C

Table 1 Maximum evaporation rates of Cr from Cr_2O_3 and $MnCr_2O_4$ for a variety of temperatures, P_{O_2}, and P_{H_2O} values
Also shown are the reduction factors (ratios) for $MnCr_2O_4$ compared with Cr_2O_3.

	Maximum Cr loss, mg/cm²/h				
	Based on Glusko(a)		Based on Ebbinghaus(b)		Reduction factor from
Temperature, °C	Cr_2O_3	$MnCr_2O_4$	Cr_2O_3	$MnCr_2O_4$	$MnCr_2O_4$
			$P_{O_2} = 0.21$, $P_{H_2O} = 0$		
600	0.0000728	0.000000766	0.0000880	0.000000927	95
700	0.00199	0.0000365	0.00236	0.0000433	55
800	0.0290	0.000832	0.0338	0.000969	35
900	0.264	0.0110	0.303	0.0126	24
1000	1.67	0.0953	1.90	0.108	18
			$P_{O_2} = 0.20$, $P_{H_2O} = 0.05$		
600	0.0140	0.000148	3.88	0.0408	95
700	0.0393	0.000718	8.82	0.161	55
800	0.113	0.00323	17.2	0.494	35
900	0.433	0.0180	30.3	1.26	24
1000	2.01	0.115	50.2	2.86	18
			$P_{O_2} = 0.10$, $P_{H_2O} = 0.20$		
600	0.0332	0.000350	9.22	0.0971	95
700	0.0898	0.00164	21.0	0.384	55
800	0.216	0.00620	40.9	1.17	35
900	0.560	0.0233	71.4	2.97	24
1000	1.80	0.102	115	6.58	18
			$P_{O_2} = 0.001$, $P_{H_2O} = 0.344$		
600	0.00181	0.0000190	0.501	0.00528	95
700	0.00487	0.0000892	1.14	0.0209	55
800	0.0116	0.000333	2.23	0.0639	35
900	0.0291	0.00121	3.92	0.163	24
1000	0.0900	0.00513	6.56	0.374	18

(a) Ref 7. (b) Ref 8

dispersive (ODS) alloy Cr-5Fe-1Y_2O_3. They obtained a rate of 8.6 μg/h with an 80 × 30 × 5 mm sample for flow rates above 1.5 L/min in air at 950 °C. This is equivalent to 1.46×10^{-4} mg/cm²/h.

4. Summary

The goal of the research described herein was to quantify the benefit from additions of Mn in alloys for SOFC components to reduce the evaporation rate of Cr. Thermodynamic calculations resulted in a maximum benefit of reducing the evaporation rate by a factor of 18 at 1000 °C to as much as a factor of 95 at 600 °C. The maximum benefit was calculated assuming sufficient Mn to form a continuous layer of $MnCr_2O_4$ on the surface of the scale. Additions of less Mn would result in a lower reduction factor.

Differing sources for the thermodynamic data for $CrO_2(OH)_2(g)$ were presented to create upper and lower bounds on predicted evaporation losses.

Table 2 Composition of experimental alloys (wt.%)

Alloy	Ni	Cr	Mn	Y
G1	74.4	24.9	0.026	0
G2	74.7	24.6	0.020	0.050
G3	74.1	24.8	0.46	0.063
G4	71.5	26.4	1.44	0.083
G5	71.6	24.3	3.49	0.130

An experimental verification of these reduction factors was attempted using long-term oxidation studies to indirectly measure the evaporation rate. Spalling of the oxide scales prevented the establishment of parabolic kinetics, so a balance in scale growth from oxidation with scale loss from evaporation

was not established. Consequently, the evaporation rates were not measured.

Future work is planned to measure the reduction factors using the transpiration method.

References

1. K. Hilpert, D. Das, M. Miller, D.H. Peck, and R. Weiß, Chromium Vapor Species over Solid Oxide Fuel Cell Interconnect Materials and Their Potential for Degradation Processes, *J. Electrochem. Soc.,* 1996, **143,** p 3642-3647
2. S.P. Jiang, J.P. Zhang, and K. Föger, Deposition of Chromium Species at Sr-Doped $LaMnO_3$ Electrodes in Solid Oxide Fuel Cells. II. Effect on O_2 Reduction Reaction, *J. Electrochem. Soc.,* 2000, **147,** p 3195-3205
3. S.P. Jiang, J.P. Zhang, L. Apateanu, and K. Föger, Deposition of Chromium Species at Sr-Doped $LaMnO_3$ Electrodes in Solid Oxide Fuel Cells. I. Mechanism and Kinetics, *J. Electrochem. Soc.,* 2000, **147,** p 4013-4022
4. O. Kubaschewski and C.B. Alcock, *Metallurgical Thermochemistry,* Vol 184, Pergamon Press, New York, 1979, p 127-131, 139-143
5. E.J. Opila, Volatility of Common Protective Oxides in High-Temperature Water Vapor: Current Understanding and Unanswered Questions, *Mater. Sci. Forum,* 2004, **461-464,** p 765-774
6. G.H. Geiger and D.R. Poirier, *Transport Phenomena in Metallurgy,* Addison-Wesley, Reading, MA, 1973, p 529-532
7. Glusko, Thermocenter of the Russian Academy of Sciences, IVTAN Association, Moscow, Russia, 1994
8. B.B. Ebbinghaus, Thermodynamics of Gas-Phase Chromium Species: The Chromium Oxides, the Chromium Oxyhydroxides, and Volatility Calculations in Waste Incineration Processes, *Combust. Flame,* 1993, **93,** p 119-137
9. IVTANTHERMO—A Thermodynamic Database and Software System for the Computer, V.S. Yungman, V.A. Medvedev, I.V. Veits, and G.A. Bergman, Ed., CRC Press, Boca Raton, Florida, 1993
10. A. Roine, *HSC Chemistry 5.11,* Outokumpu Research Oy, Pori, Finland, 2002
11. C. Gindorf, L. Singheiser, K. Hilpert, M. Schroeder, M. Martin, H. Greiner, and F. Richter, Chromium Vaporization from Metallic Interconnect and Retention by Perovskite Layers, *Solid Oxide Fuel Cells (SOFC VI), Proc. 6th Int. Symp.,* S.C. Singhal and M. Dokiya, Ed., Electrochemical Society, Pennington, New Jersey, 1999, Vol 99-19, p 774-782
12. E.J. Opila, NASA Glenn Research Center, Cleveland, Ohio, private communication, 2004
13. K.T. Jacob and K. Fitzner, Ion-Exchange Equilibria between (Mn,Co)O Solid Solution and $(Mn,Co)Cr_2O_4$ and $(Mn,Co)Al_2O_4$ Spinel Solid Solutions at 1100 °C, *J. Mater. Sci.,* 1977, **12,** p 481-488
14. J.V. Biggers, "Experimental Determination of Some Thermodynamic Properties of Oxide Solid Solutions Containing MnO and CoO," Ph.D. Thesis, Pennsylvania State University, University Park, Pennsylvania, 1966
15. N. Koc, "Activity-Composition Relations in $MnCr_2O_4$-$CoCr_2O_4$ Solid Solutions and Stabilities of $MnCr_2O_4$ and $CoCr_2O_4$," Ph.D. Thesis, Middle East Technical University, Ankara, Turkey, 1993
16. H.-T.T. Tsai and A. Muan, Activity-Composition Relations in $FeCr_2O_4$-$FeAl_2O_4$ and $MnCr_2O_4$-$MnAl_2O_4$ Solid Solutions at 1500° and 1600 °C, *J. Am. Ceram. Soc.,* 1992, **75,** p 1407-1411